Author Queries

JOB NUMBER: 527838

JOURNAL: GCMB

Q1 Please check the affiliation details ‘a and c’.

Q2 The reference citation ‘Appanaboyina et al. (2007)’ has been changed to ‘Appanaboyina et al. (2008)’ as per the reference list. Please check and confirm.

Q3 We have made a change to this sentence. Please review our edit.

Q4 Please confirm our edit of the word ‘modulus’ to ‘ratio’ in this sentence.

Computer Methods in Biomechanics and Biomedical Engineering
Vol. 00, No. 0, 2010, 1–9

Taylor & Francis
Taylor & Francis Group

Deployment of self-expandable stents in aneurysmatic cerebral vessels: comparison of different computational approaches for interventional planning

A. Bernardini[a,b1], I. Larrabide[a,b]*, L. Petrini[c2], G. Pennati[c3], E. Flore[a,b4], M. Kim[a,b5] and A.F. Frangi[a,b,d6]

[a]*Center for Computational Imaging and Simulation Technologies in Biomedicine (CISTIB), Universitat Pompeu Fabra (UPF), C/Roc Boronat 138, 08018 Barcelona, Spain;* [b]*Networking Center on Biomedical Research (CIBER-BBN), Barcelona, Spain;* [c]*Laboratory of Biological Structure Mechanics, Politecnico di Milano, Piazza Leonardo da Vinci 32, 20133 Milano, Italy;* [d]*Institució Catalana de Recerca i Estudis Avançats (ICREA), Barcelona, Spain*

(*Received 28 July 2010; final version received 25 September 2010*)

In the last few years, there has been a growing focus on faster computational methods to support clinicians in planning stenting procedures. This study investigates the possibility of introducing computational approximations in modelling stent deployment in aneurysmatic cerebral vessels to achieve simulations compatible with the constraints of real clinical workflows. The release of a self-expandable stent in a simplified aneurysmatic vessel was modelled in four different initial positions. Six progressively simplified modelling approaches (based on Finite Element method and Fast Virtual Stenting – FVS) have been used. Comparing accuracy of the results, the final configuration of the stent is more affected by neglecting mechanical properties of materials (FVS) than by adopting 1D instead of 3D stent models. Nevertheless, the differences showed are acceptable compared to those achieved by considering different stent initial positions. Regarding computational costs, simulations involving 1D stent features are the only ones feasible in clinical context.

Keywords: fast virtual stenting method; finite element method; shape memory alloy; nitinol; stent

Nomenclature

FE	Finite element
FVS	Fast virtual stenting
RD	ring distance (mm)
R	radius of the vessel (mm)
Δd	distance between two configurations (mm)
ρ	curvature radius of the vessel (mm)
λ	elongation (–)
ε	strain (–)
σ	stress (MPa)

1. Introduction

An intracranial cerebral aneurysm is an out bulge resulting from a cerebrovascular disorder whereby a locally weakened vessel wall expands like a balloon. Typically, these can be found at the Circle of Willis, around or at the bifurcations. The rupture of an aneurysm will most likely cause a subarachnoid haemorrhage with a high mortality and morbidity rate (Brach 2009). Nowadays, cerebral aneurysms are often detected before rupture, thanks to the advances and ready availability of non-invasive medical imaging techniques. When an unruptured cerebral aneurysm is detected, the physician has to rapidly decide whether to treat it preventively or not and, in case of treatment, the neurosurgeon or interventional radiologist has to choose from a number of alternative options: surgical treatment (clipping) or minimally invasive therapies (coils or stents) (Ringer et al. 2001). Concerning minimally invasive solutions, several studies have indicated that positioning a low-porous self-expandable stent in the cerebral vessel at the aneurysm neck lessens the flow into the aneurysmatic sac. The consequent creation of areas with stagnant flow and low shear rates may induce thrombus formation inside the aneurysm and decrease its risk of rupture (Lieber et al. 2002; Baráth et al. 2004).

A number of papers (Kim et al. 2007; Appanaboyina et al. 2008; Kim et al. 2008; Liou et al. 2008; Appanaboyina et al. 2009; Fu et al. 2010) have studied the influence of stenting procedures from a fluid dynamic point of view. These papers showed that aneurismal flow mainly depends on the post release stent configuration. In turn, the released configuration depends on both the design and orientation of the stent and the main anatomical features, such as vessel curvature and diameter and aneurysm neck dimension.

The possibility of estimating the post release stent configuration in patient-specific geometry, and its effects on local blood flow, would be welcomed by interventional neuroradiologists for both treatment planning and training purposes. The interest in numerical tools, which support clinician decisions, has increased over the last few years.

*Corresponding author. Email: ignacio.larrabide@upf.edu

ISSN 1025-5842 print/ISSN 1476-8259 online

DOI: 10.1080/10255842.2010.527838
http://www.informaworld.com

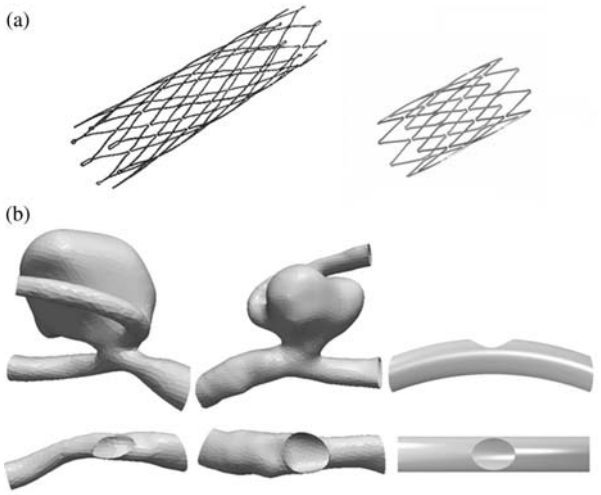

Figure 1. Geometries adopted for stent and aneurysmatic cerebral vessel models. (a) μ-CT scan reconstruction of the neuroform stent (Boston Scientific) with eight rings (left) and CAD model with four rings (right). It has a nominal diameter of 4.5 mm, a total length of 10 mm and a radial thickness of 0.08 mm; the rings are connected by links. The struts have a length of 2.43 mm and a width of 0.1 mm, while the links have a length of 0.26 mm and a width of 0.34 mm. (b) 3DRA reconstruction of two cerebral aneurysms from @neurIST (Frangi et al. 2007) database (at the Sylvian Bifurcation and Middle Cerebral Artery – left) and simplified computational model (right) having a wall thickness of 0.3 mm, a radius $R = 1.8$ mm and a curvature radius $\rho = 30$ mm and an elliptical aneurysm neck 4.5×3.24 mm.

Rapid advances in technology and the demand for improved patient safety have led to an increased use of simulation technologies in medicine (Dawson et al. 2007; Sarker and Patel 2007; Tsang et al. 2008). Such support becomes increasingly important when, as in the case of endovascular treatment of cerebral aneurysms, the number of previously treated patients is limited (i.e. no large databases of cases are available).

The most advanced techniques for the simulation of intracranial aneurysm stenting were illustrated in a recent study (Appanaboyina et al. 2009). The simulation of flow alteration caused by different endovascular devices requires overcoming a number of challenging technical problems, including the simulation of stent deployment inside patient-specific vascular models, the computation of pulsatile flows around deployed devices and comparison of the performances of different treatment options (e.g. stent design or stent positioning). All these technical problems should be addressed realistically and efficiently.

Presently, simple approaches based on deformable meshes (Larrabide et al. 2010) are used to virtually deploy stent models into patient-specific vascular models of aneurysmatic regions. However, such an approach neglects the structural mechanics of the stents and its interaction with the parent artery due to the force exerted by devices. Both these effects influence the characteristics of vessel–stent conformability and should be incorporated for a more accurate representation of the stent geometry in its deployed state. In this regard, Finite element (FE) analysis could be used to study the mechanical behaviour of stents and their interaction with the vascular wall during its deployment. Actually, while an extensive application of FE modelling for simulating the treatment of vessel stenoses can be found in the literature (Migliavacca et al. 2004; Wu et al. 2007; De Beule et al. 2008; Gijsen et al. 2008; Early et al. 2009; Mortier et al. 2010), to date the amount of similar studies on cerebral aneurysm treatment has been very limited. In fact, the Finite Element method (FEM) allows very complex models to be developed, including high non-linearity due to material properties (for instance, Holzapfel et al. 2005, for the biomechanics of coronary arteries, and Petrini et al. 2005, for the material properties of the stent) and kinematics, which facilitate accurate description of the stenting procedure. On the other hand, the high-computational cost of these models makes their use not feasible in the operating theatre.

In the present work, we investigate the possibility of introducing suitable approximations in the computational models to progressively reduce their complexity and computational time and to allow the use of virtual stenting as a supporting tool during the cerebral aneurysm treatment. There are two main questions which have to be answered: (i) how much do the stent and vessel wall models have to be simplified in order to reduce the computational time to one suitable for the clinical environment? (ii) What information do we lose by simplifying these models and what is the significance? In this regard, it is worth noting that during the interventional procedure a number of variables cannot be precisely controlled, such as the exact position of the stent within the vessel. This issue needs to be taken into account when evaluating the clinical applicability of different computational approaches.

2. Materials and Methods

2.1 Geometry models and material properties

A self-expanding stent, made of a nickel–titanium alloy and resembling the neuroform stent (Boston Scientific, Natick, MA, USA), was considered. Its geometry was obtained from a μ-CT scan of the real stent (Radaelli et al. 2008) (Figure 1(a)). The stent is expanded within an idealised vessel geometry, similar to those of cerebral aneurysms (Figure 1(b)), where only the elliptic aneurysm orifice is reproduced. The vessel and stent model geometries are created using the commercial CAD software Rhinoceros 4.0 Evaluation (McNeel & Associates, Indianapolis, IN, USA).

Different modelling approaches are compared, characterised by an increasing level of simplification in terms of numerical method (FEM to deformable mesh), geometry

Table 1. Main features of the analysed cases.

Case	FE3H	FE3E	FE3R	FE1H	FE1R	FVS
Method	FEM	FEM	FEM	FEM	FEM	FVS
Strut and link description	3D	3D	3D	1D	1D	1D
Stent material (see Figure 3)	Nitinol	Nitinol	Nitinol	Nitinol	Nitinol	–
Stent mesh element	Eight-node brick	Eight-node brick	Eight-node brick	Two-node linear beam	Two-node linear beam	Two-simplex mesh
Stent N elements	87,984	87,984	87,984	393	393	640 nodes
Vessel material (see Figure 3)	Hyperelastic	Linear elastic	Rigid body	Hyperelastic	Rigid body	Rigid body
Vessel mesh element	Three-node shell	Three-node shell	Three-node shell	Three-node shell	Three-node shell	–
Vessel N elements	58,323	58,323	58,323	4273	4273	–
Interaction stent–vessel	Soft exponential	Soft exponential	Soft exponential	Soft exponential	Soft exponential	Soft expanding force

(3D to 1D) and material properties. Table 1 resumes in detail the features of the six cases, from the most complex (case FE3H) to the simplest [case fast virtual stenting (FVS)].

Considering the five cases based on FEM, both 3D and 1D models are adopted for the stent, using eight-node brick elements or two-node linear beam elements for the model discretisation, respectively. Figure 2 shows the simplification in stent geometry with struts and links modelled as 1D-elements. A total of 64 nodes, having the same geometrical coordinates in the two meshes, are selected as reference points (details in Figure 2). The ability of nickel–titanium alloy to recover the original shape (pseudo-elastic effect) is described by the use of a previously developed user subroutine (Auricchio and Petrini 2004). Average values are used for material parameters (Migliavacca et al. 2004; Wu et al. 2007), since the specific properties for the neuroform stent are not available. The corresponding uniaxial stress–strain curve is depicted in Figure 3 (left). Concerning the vessel wall modelling, a single homogeneous layer is considered and discretised by a mesh of three-node shell elements. Three different constitutive models are chosen to describe the mechanical behaviour of the wall: a hyperelastic isotropic model whose parameters are derived from experimental data on cerebral vessels (Monson et al. 2006), a linear elastic isotropic model with Young's modulus corresponding to the initial behaviour ($\lambda < 1.09$) of the hyperelastic curve (Figure 3 – right) and a rigid body model.

Finally, the FVS method is used in the last case. No material property definitions are required by this methodology, and only geometrical information about the stent is needed, as described in Section 2.2. In FVS, the stent geometry is created by defining, over a subset of points constituting a simplex mesh (Montagnat and Delingette 1998), the sets of nodes corresponding to the extremities of the struts (reference points) and their connectivity. Accordingly, the same unidimensional geometry used for 1D FEM is considered for the stent, whereas the vessel wall is described as a rigid body.

2.2 Simulations

Structural FE analyses were performed by means of the commercial code ABAQUS/Standard 6.8EF (Simulia Corp., Providence, RI, USA). To simulate the stent release, two steps were defined: the crimping of the stent and its self-expansion until its interaction with the vessel wall. The crimping procedure was simulated by uniformly applying a negative radial displacement to the nodes of the internal surface of the stent up to when the stent resides completely inside the vessel. After crimping, all constraints in the radial direction are removed allowing the free expansion of the stent until it contacts the vessel wall. In order to prevent rigid motions of the vessel and stent, the vessel was fixed at its endings, the reference points of the stent were constrained

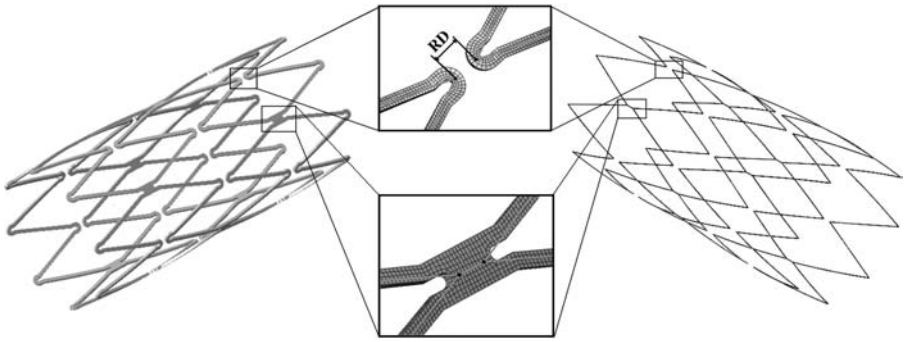

Figure 2. FEM 3D and 1D models of the stent. In the middle, some details showing the approximation of 1D model (red lines) and reference points (bold dots). The value of the RD is 0.26 mm.

tangentially and three reference points of the central section were constrained axially. A soft exponential frictionless interaction was adopted to manage the contact between the stent and the vessel wall (ABAQUS Theory Manual 2008).

The FVS algorithm uses the constrained deformable simplex model proposed by Larrabide et al. (2010). Firstly, the stent geometry is generated in a crimped configuration (Figure 4). Then, the stent is deployed according to a second-order differential equation, defined for each point of the simplex mesh. This equation takes into account constraining forces which represent the internal (related to the simplex mesh smoothness) and stent-shaped constraining forces (fictitious, related to the strut length), and an external force, which expands the mesh towards the vessel wall. Finally, the interaction between the stent and wall is defined by the interruption of the expanding force, when mesh points reach the vessel wall.

The six computational approaches are applied to four different neck-stent relative initial positions (posA, posB, posC and posD), corresponding to various small translations and/or rotations of the stent (Figure 5).

All the simulations were executed on Personal Computer Intel(R) Core(TM)2 Quad CPU Q9550 @ 2.83 GHz with 8.00 GB of RAM.

2.3 Data analysis

The expanded configuration of the case FE3H (see, Table 1 and Figure 6) is selected as the gold standard, as it represents the most detailed and complex model. The reliability of the other, more simplified, methods (cases FE3E to FVS) is assessed by comparing the final expanded stent configuration. Namely, the distances (Δd) between the reference points in the case FE3H and the corresponding reference points in each of the other cases are calculated and normalised with respect to the vessel radius (R). Moreover, a toroidal coordinate system, applied to the curved vessel, is also used to compute the radial and the circumferential components of these normalised distances. All these results are evaluated for the four relative initial neck-stent positions.

Since the part of the stent lying over the aneurysm neck is expected to have the greatest impact on the aneurysm

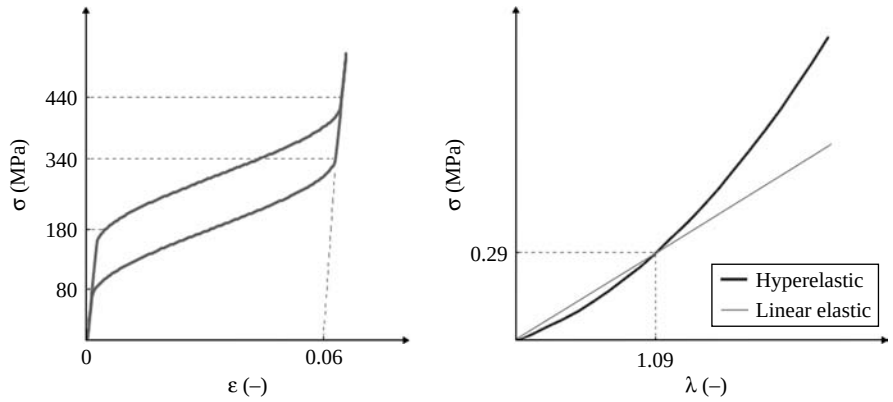

Figure 3. Pseudo-elastic model for nickel–titanium alloy of the stent (left) and elastic models adopted for the vessel wall material (right). The hyperelastic constitutive law is based on a second-order reduced polynomial strain energy density function characterised by the following parameters: $\nu = 0.49$; D1 = D2 = 0, C10 = 3.3096, C20 = 0.6353, C01 = −3.0197, C11 = 0.5814, C02 = −0.2745. Q4 The linear elastic constitutive law is characterised by Young's modulus of 3.2 MPa and Poisson's ratio of 0.49.

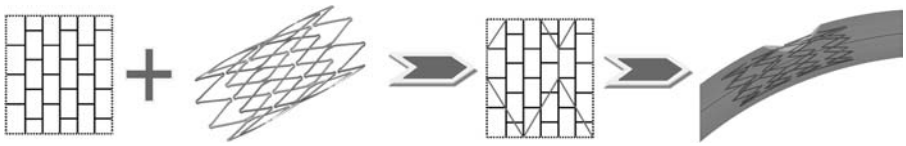

Figure 4. FVS methodology. Once the stent geometry is created in the initial undeformed configuration over a subset of points constituting the simplex mesh, the simplex mesh is deformed to obtain a curved tube fully contained within the vessel and having its axis along the vessel centreline.

haemodynamics (Kim et al. 2008), particular attention is paid to analysing the results in this area. Accordingly, two additional quantities are evaluated: the strut protrusion towards the aneurysm and the deformed ring distance (RD). The former is calculated as the difference between the radial coordinate of each reference point and the deformed vessel radius. The latter is evaluated as the projection on the neck plane of the distance between the ends of the struts of different adjacent rings. Both quantities are normalised to the value of R.

Finally, even though the run-time is platform specific, the CPU time is used as an indication of the computational cost of running the simulations with the different modelling approaches.

3. Results

Figure 6 shows the configuration of the stent–vessel system after deployment for all six investigated cases, corresponding to posA initial positioning. Primary analysis of the different configurations allows for some qualitative considerations: (i) simulations accounting for a deformable vessel wall (FE3H, FE3E and FE1H) result in a straightening of the vessel and an enlargement of the neck (creating a more circular shape); (ii) the simplification from 3D to 1D model in the corresponding FE models (FE3H vs. FE1H and FE3R vs. FE1R) does not significantly influence the final configuration; (iii) FVS shows the most stent foreshortening. Similar considerations can be drawn for the other initial positions (results not reported).

A quantitative comparison – in terms of normalised distance ($\Delta d/R$) between the positions of the reference points in case of FE3H and in all other cases – is plotted in Figure 7 (top panel) for all the studied initial positions. The performances of various computational approaches are consistent throughout initial positions and confirm previous qualitative analysis: the deployed stents in cases FE3E and FE1H (deformable vessel walls) are very similar to that of case FE3H showing very low differences (mean and third quartile distances lower than 2%, maximum distances lower than 6%), whereas higher differences occur disregarding vessel deformability. In particular, cases FE3R and FE1R show maximum distances up to 9%,

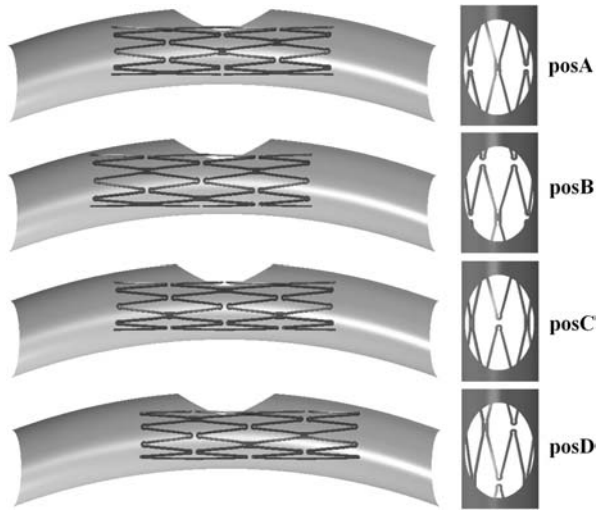

Figure 5. Different model configurations after stent crimping, which mimics the uncertainty in stent positioning with respect to the aneurysm neck. posB and posD translated of ± 1.1 mm, and posC and posD rotated to 45° with respect to posA.

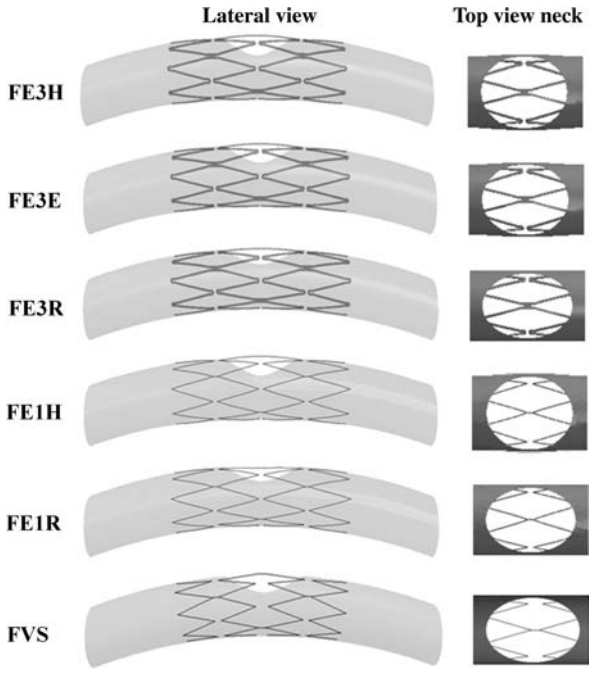

Figure 6. Configuration of the stent after its deployment (in position posA) into the vessel under the six modelling strategies: lateral view of the section of the vessel and top view of the neck area. Position posA.

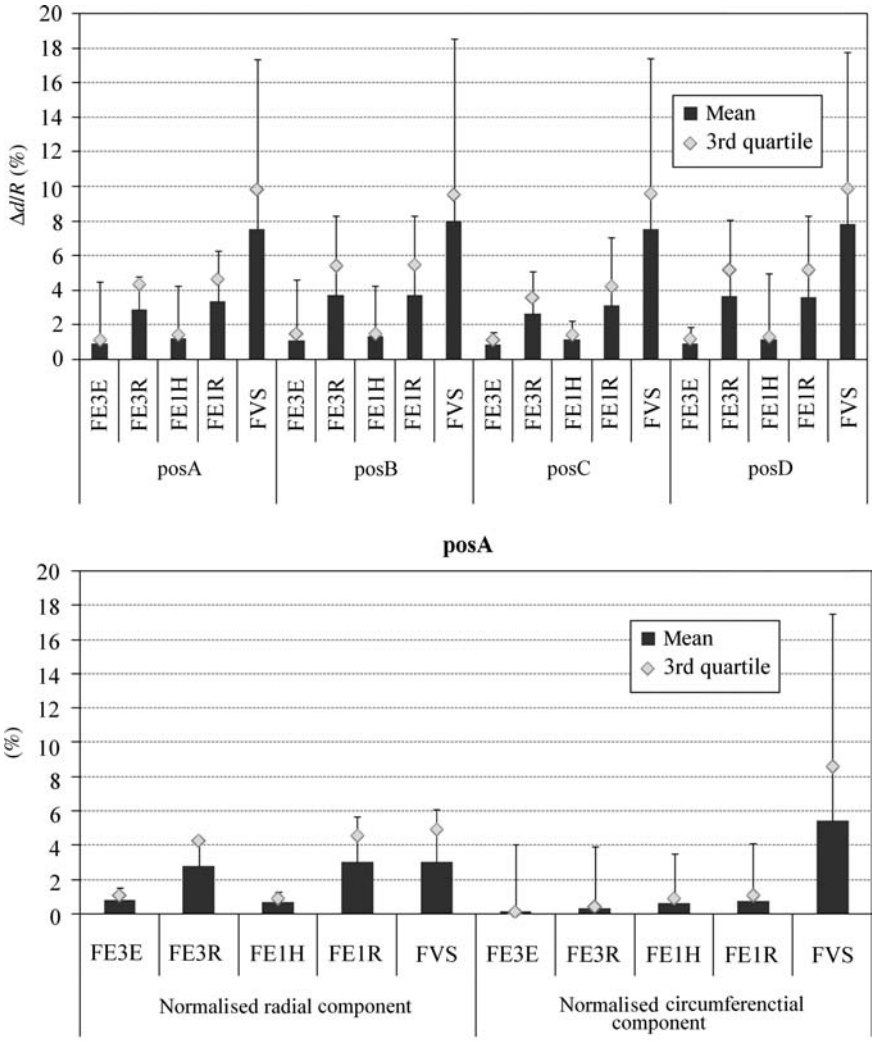

Figure 7. Relative differences (in %) in the locations of the reference nodes of deployed stents for different modelling strategies compared to FE3H. Top panel: normalised distance ($\Delta d/R$) for all the positions (from posA to posD). Bottom panel: radial and circumferential components of the normalised distances for the sole position posA. Mean, third quartile and maximum differences are reported.

while for FVS the differences in predicting the deployed stent geometry can rise up to 20%.

For a deeper investigation of the differences between the models, in Figure 7 (bottom panel) the differences calculated in terms of normalised radial and circumferential components of $\Delta d/R$ are plotted for a single initial position (posA), although similar results are found for other positions. Considering third quartile values, radial differences are around 1% in both cases FE3E and FE1H, becoming around 5% in both cases FE3R and FE1R. The FVS model behaves quite similarly to the case FE1R: mean differences are almost the same, even if third quartile and maximum are higher for FVS. All the FE case differences are lower than 1% in the circumferential direction. Compared to all FE models, the FVS approach produces quite larger differences (mean and third quartile higher than 5%, maximum higher than 17%), in agreement with previously noticed excessive stent foreshortening.

Figure 8 focuses on the behaviour of the stent portion covering the aneurysm neck. Strut protrusion is very sensitive to initial positioning and the adopted numerical approach: namely, in position posA models FE3R and FE1R do not show any protrusion, while other cases have similar values (lower than 5%), in position posD all the models but FVS gives similar results (9–16%), while in positions posB and posC the protrusion varies strongly from one case to the other (ranging from 2 to 23%). On the other hand, the deformed RD has a range of 14–21% for all the FE cases in all the positions, whereas FVS shows a value of around 40%.

Finally, the computational cost of the models is compared in Figure 9 (mean values between the four positions). There is a large difference between FE3H and

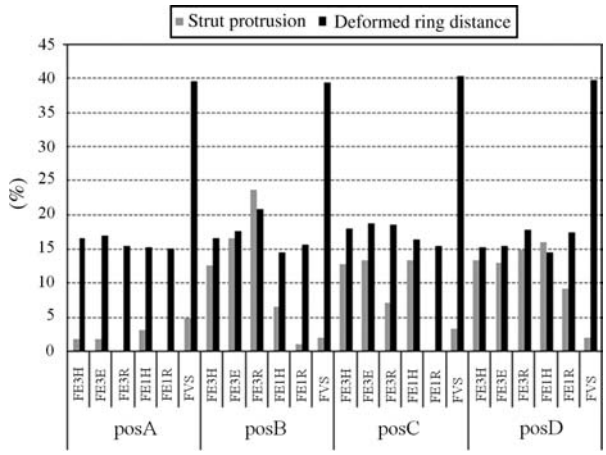

Figure 8. Stent protrusion and deformed RD in the neck zone for all the investigated models.

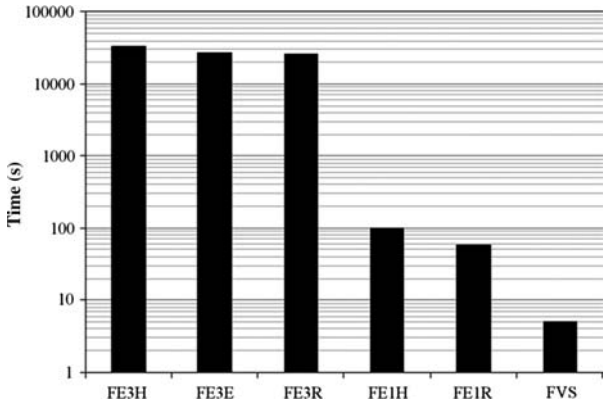

Figure 9. Computational cost of the different models.

FVS simulation times (32,727 vs. 5 s). Disregarding the material properties of the vessel wall leads to an increase of 6200 s from case FE3H to FE3R (~20% reduction) and of 40 s from cases FE1H to FE1R (~40% reduction). However, the most significant gain in computational time (~300%) is obtained by simplifying the geometry of the stent from 3D to 1D: from 32,727 s (FE3H) to 98 s (FE1H). The less expensive simulations are those based on FVS, which run in about 5 s.

4. Discussion

The present study was performed to evaluate the possibility of simplifying the computational approach to the stenting procedure to achieve a clinically suitable computational time, to identify where information is lost and to quantify its relevance.

The results of this study highlight that

- neglecting the mechanical properties of the stent is the main reason for differences in performance both globally and locally (neck area) across different models;
- neglecting the vessel deformability (as in FE3R and FE1R) also influences the results, implying differences of around 6% across models, mainly in the radial components;
- considering 3D or 1D struts and link models does not induce significant differences in the final configuration of the stent;
- considering 1D models instead of 3D models allows reduction in the computational cost from 32,727 s (3D FEM) to 98 s (1D FEM), down to 5 s (FVS).

During the intervention, the orientation of the stent in the vessel is not precisely controlled by the interventional radiologist. Even if the intention of the interventionist is to position the stent as in position posA, the three other investigated positions (from posB to posD, see Figure 5) could be obtained. We used the four FE3H positions to reproduce the variability in the stent location during its implantation. The variability of 35% in the deployed configurations observed in the four FE3H results suggests that all the investigated computational approaches, showing differences lower than 25% in predicting the deployed stent configuration, could provide useful indications from a clinical point of view. Furthermore, simulating the deployment of the neuroform-like stent may be considered a worst-case scenario for the benchmarked virtual stenting tools, since this stent shows an open-cell design, which highlights the differences in release configurations in the neck region.

With respect to the computational cost of the virtual stenting process in relation to its clinical acceptance, we have to remember that virtual deployment is just one step of interventional planning for intracranial aneurysm stenting as a whole. Once we have optimised virtual deployment, other steps (e.g. computational haemodynamic simulations considering the deployed device) will now be the limiting factors (Appanaboyina et al. 2009). In general, a tool for virtual stenting should allow clinicians to compare different treatment alternatives and select the most effective one without delaying the current clinical workflow or limiting the planning throughput. Note that this process, however, could still consume a few hours in the case of elective patients.

In conclusion, the FE1H approach may be a good compromise as a simplified model for the stenting procedure with no loss of detailed features. Also, if in addition to computational costs, ease of implementation, automation of the process (allowing the clinician direct access without the presence of an expert) and clinical acceptance are important requirements, the FVS approach should be recommended for virtual stenting in interventional planning.

The main limitation of the present study is the use of a single and simplified curved geometry for the vessel. Although more complex geometries are associated with patient-specific cases of intracranial aneurysms, the idealised

anatomy is acceptable as the aim of this study is to compare different numerical approaches to the same model. It is to be expected that by increasing the complexity of the vessel geometry, a better description of the stent–wall interaction is required. Therefore, the differences in the final deployed configuration of the stent and the computational cost could be higher. Nevertheless, to the best of our understanding there is no reason to believe that the relative performance of the different modelling techniques should not remain the same. Furthermore, in our experiments we neglected the description of the dome of the aneurysm. We based this assumption on the results of preliminary simulations, in which the stents were deployed in the deformable vessels with and without the dome. Comparing the final configuration of the stents, we found the mean difference to be less than 0.3% of the vessel radius for the vessel without the dome. Another limitation concerns the choice of the case FE3H as a gold standard, when more refined constitutive vascular models are currently under development (e.g. Holzapfel et al. 2005). For the material properties of the vessel, we adopted a homogeneous hyperelastic isotropic description, because in case of self-expandable stents for cerebral aneurysm treatment, used without balloon, the vessel wall works as a constraint to the stent expansion. Therefore, for the purpose of this study, we found that the global stiffness of the vessel is more important than a detailed description of material properties. In fact, we found that the mean difference between the two elastic models (FE3H and FE3E) is lower than 2%.

Acknowledgements

This work was partially supported within the CENIT CDTEAM (2006–2009) and cvREMOD (2010–2012) projects funded by the Spanish MICINN-CDTI, and partly within the framework of the @neurIST Integrated Project (IST-2005-027703), which is co-financed by the European Commission within the IST Program of Sixth Framework Program. Authors are very grateful to Stefano Morlacchi for the technical support in simulations and to Cecily Doyle for the support in language revision of this manuscript.

Conflict of interest: Authors declare that they have no conflict of interests.

Notes

1. Email: abernardini@cistib.upf.edu
2. Email: lorenza.petrini@polimi.it
3. Email: giancarlo.pennati@polimi.it
4. Email: eleonora.flore@gmail.com
5. Email: m.kim@surrey.ac.uk
6. Email: alejandro.frangi@upf.edu

References

ABAQUS Theory Manual. 2008. Version 6.8EF. Pawtucket, RI: Hibbit, Karlsson and Sorensen, Inc.

Appanaboyina S, Mut F, Löhner R, Putman CM, Cebral JR. 2008. Computational fluid dynamics of stented intracranial aneurysms using adaptive embedded unstructured grids. Int J Numer Methods Fluids. 57:475–493.

Appanaboyina S, Mut F, Löhner R, Putman CM, Cebral JR. 2009. Simulation of intracranial aneurysm stenting: techniques and challenges. Comput Methods Appl Mech Eng. 198:3567–3582.

Auricchio F, Petrini L. 2004. A three-dimensional model describing stress-temperature induced solid phase transformations: solution algorithm and boundary value problems. Int J Numer Methods Eng. 61:807–836.

Baráth K, Cassot F, Rüfenacht DA, Fasel JH. 2004. Anatomically shaped internal carotid artery aneurysm *in vitro* model for flow analysis to evaluate stent effect. Am J Neuroradiol. 25(10):1750–1759.

Brach RF. 2009. Coil or clip? Current trends in the treatment of intracranial aneurysms. J Am Acad Phys Assist. 22(2):37–38, 40–42.

Dawson DL, Meyer J, Lee ES, Pevec WC. 2007. Training with simulation improves residents' endovascular procedure skills. J Vasc Surg. 45:149–154.

De Beule M, Mortier P, Carlier SG, Verhegghe B, Van Impe R, Verdonck P. 2008. Realistic finite element-based stent design: the impact of balloon folding. J Biomech. 41(2):383–389.

Early M, Lally C, Prendergast PJ, Kelly DJ. 2009. Stresses in peripheral arteries following stent placement: a finite element analysis. Comput Methods Biomech Biomed Eng. 12(1):25–33.

Frangi AF, Hose DR, Ruefenacht DA. 2007. The @neurIST project: towards understanding cerebral aneurysms. Newsletter in SPIE newsroom. DOI: 10.1117/2.1200706.0782.

Fu W, Gu Z, Meng X, Chu B, Qiao A. 2010. Numerical simulation of hemodynamics in stented internal carotid aneurysm based on patient-specific model. J Biomech. 43:1337–1342.

Gijsen FJH, Migliavacca F, Schievano S, Socci L, Petrini L, Thury A, Wentzel JJ, Van der Steen AFW, Serruys PWS, Dubini G. 2008. Simulation of stent deployment in a realistic human coronary artery. Biomed Eng OnLine. 6:7–23.

Holzapfel GA, Sommer G, Gasser CT, Regitnig P. 2005. Determination of layer-specific mechanical properties of human coronary arteries with nonatherosclerotic intimal thickening and related constitutive modelling. Am J Physiol Heart Circ Physiol. 289(5):2048–2058.

Kim M, Levy EI, Meng H, Hopkins LN. 2007. Quantification of hemodynamic changes induced by virtual placement of multiple stents across a wide-necked basilar trunk aneurysm. Neurosurgery. 61(6):1305–1313.

Kim M, Taulbee DB, Tremmel M, Meng H. 2008. Comparison of two stents in modifying cerebral aneurysm hemodynamics. Ann Biomed Eng. 36:726–741.

Larrabide I, Kim M, Augsburger L, Villa-Uriol MC, Rüfenacht D, Frangi AF. 2010. Fast virtual deployment of self-expandable stents: method and *in-vitro* validation for intracranial aneurysmal stenting. Med Image Anal. in press, DOI: 10.1016/j.media.2010.04.009.

Lieber BB, Livescu V, Hopkins LN, Wakhloo AK. 2002. Particle image velocimetry assessment of stent design influence on intra-aneurysmal flow. Ann Biomed Eng. 30:768–777.

Liou TM, Li YC, Wang TC. 2008. Hemodynamics altered by placing helix stents in an aneurysm at a 45° angle to the curved vessel. Phys Med Biol. 53:3763–3776.

Migliavacca F, Petrini L, Massarotti P, Schievano S, Auricchio F, Dubini G. 2004. Stainless and shape memory alloy coronary

stents: a computational study on the interaction with the vascular wall. Biomech Model Mechanobiol. 2:205–217.

Monson KL, Barbaro NM, Manley GT. 2006. Multiaxial response of human cerebral arteries. Paper presented at: The 2006 Annual Meeting of the American Society of Biomechanics; Virginia Polytechnic Institute and State University, Blacksburg, VA.

Montagnat J, Delingette H. 1998. Globally constrained deformable models for 3D object reconstruction. Signal Process. 71(2):173–186.

Mortier P, Holzapfel GA, De Beule M, Van Loo D, Taeymans Y, Segers P, Verdonck P, Verhegghe B. 2010. A novel simulation strategy for stent insertion and deployment in curved coronary bifurcations: comparison of three drug-eluting stents. Ann Biomed Eng. 38(1):88–99.

Petrini L, Migliavacca F, Massarotti P, Schievano S, Dubini G, Auricchio F. 2005. Computational studies of shape memory alloy behaviour in biomedical applications. J Biomech Eng. 127(4):716–725.

Radaelli AG, Augsburger L, Cebral JR, Ohta M, Rufenacht DA, Balossino R, Benndorf G, Hose DR, Marzo A, Metcalfe R, et al. 2008. Reproducibility of haemodynamical simulations in a subject-specific stented aneurysm mode – a report on the virtual intracranial stenting challenge. J Biomech. 41(10):2069–2081.

Ringer A, Lopes D, Boulos A, Guterman L, Hopkins L. 2001. Current techniques for endovascular treatment of intracranial aneurysms. Semin Cerebrovasc Dis Stroke. 1(1):39–51.

Sarker SK, Patel B. 2007. Simulation and surgical training. Int J Clin Pract. 61:2120–2125.

Tsang JS, Naughton PA, Leong S, Hill AD, Kelly CJ, Leahy AL. 2008. Virtual reality simulation in endovascular surgical training. Surgeon. 4(8):214–220.

Wu W, Qi M, Liu XP, Yang DZ, Wang WQ. 2007. Delivery and release of nitinol stent in carotid artery and their interactions: a finite element analysis. J Biomech. 40(13):3034–3040.